ELSEVIER

Polymer 42 (2001) 7809–7817

polymer

www.elsevier.nl/locate/polymer

Molecular dynamics simulations and structural comparisons of amorphous poly(ethylene oxide) and poly(ethylenimine) models

Haitao Dong, Jin-Kee Hyun, Curtis Durham, Ralph A. Wheeler*

Department of Chemistry and Biochemistry, University of Oklahoma, 620 Parrington Oval, Room 208, Norman, OK 73019, USA

Received 5 December 2000; received in revised form 16 March 2001; accepted 16 March 2001

Abstract

Poly(ethylene oxide) (or PEO, $(-CH_2CH_2O-)_n$) and poly(ethylenimine) (PEI, $(-CH_2CH_2NH-)_n$) have been suggested as host polymers for solid polymer electrolytes in high energy-density batteries. Four repeat-unit models for amorphous PEO and PEI ($CH_3X(CH_2CH_2X)_4CH_3$, $X = O$ in PEO-4 and NH in PEI-4) were studied by molecular dynamics (MD) simulations at 300 K. Analysis of average chain dimensions indicates that PEI-4 adopts a more compact structure than PEO-4. The characteristic ratios of 4.9 ± 0.1 for PEO-4 and 3.1 ± 0.1 for PEI-4 are consistent with experiment and with theoretical predictions. Dihedral angles along the C—*X*—C—C atom sequence favor the trans (T) conformation while the *X*—C—C—*X* sequence favors the gauche (G) conformation for both models. The TGT conformation along the C—*X*—C—C—*X*—C sequence is found to have the largest population, $59 \pm 3\%$ in PEO-4 and $66 \pm 2\%$ in PEI-4. The TTT conformation becomes much less populous in PEI-4 ($1.6 \pm 0.4\%$) than in PEO-4 ($20 \pm 2\%$) while the TGG conformation has a larger population in PEI-4 ($24 \pm 2\%$) than in PEO-4 ($6 \pm 2\%$). Radial distribution function analysis reveals that intra-chain H-bonds exist between two adjacent NH groups of PEI-4 chains. All intra-chain H-bonds are found to be nonlinear and longer than typical H-bonds. These results are consistent with an ab initio study of a methyl capped monomer of PEI, dimethylethylenediamine. Inter-chain H-bonds are also found in the amorphous state of PEI-4 and appear to be more like typical linear H-bonds. Only 5.6% PEO-4 and 8.2% PEI-4 chains are found to be in the helical form and an insignificantly amount of PEI-4 is found in double-stranded helices in amorphous PEI-4. © 2001 Published by Elsevier Science Ltd.

Keywords: Molecular dynamics; Poly(ethylene oxide); Poly(ethylenimine)

1. Introduction

The prospect of high energy-density batteries has been greatly improved by the application of solid polymer electrolytes (SPE) because of the polymeric materials' mechanical properties. A candidate polymer matrix should have strong enough interactions with ions to dissolve and dissociate salts into the polymer matrix [1]. NMR evidence has shown that ion movement takes place mainly in an amorphous phase in polymers [2], which is generally present at temperatures above the glass transition temperature. When a polymer system is above this temperature, local motion of polymer chains is no longer prohibited and can become associated with ion movement. Therefore, SPE and SPE-salt complexes with glass transition temperatures at or below ambient temperatures are desirable.

It has been more than 20 years since poly(ethylene oxide) (PEO, $(-CH_2CH_2O-)_n$) was first suggested as one possible polymer matrix [3]. The melting point of crystalline PEO is 338 K, and due to the regularity of the linear structure of PEO, its crystallinity can be as high as 85% [4]. X-ray diffraction studies have revealed that linear PEO adopts a (7/2) helical structure, indicating seven repeat units and two turns per crystal period [5]. The glass transition temperature of amorphous PEO is well below room temperature, at approximately 213 K [4]. The strong interactions between the electronegative ether oxygen and salt cations enable PEO to dissolve a variety of inorganic salts. PEO has therefore become a common host polymer matrix in high energy-density batteries. In fact, PEO and PEO based SPEs have been subjected to intensive study in recent years.

Structural properties of polymer matrices are one important aspect of a full understanding of ionic conductivity mechanisms in the SPEs. Molecular dynamics (MD) simulations have shown their power to represent real systems and provide insight into molecular structures [6–9]. An MD simulation of a model for crystalline PEO including 16 14-repeat unit chains in eight crystallographic cells ($2 \times 2 \times 2$) was carried out at 300 K and the equilibrium structure was compared with the X-ray crystal structure [6]. The good agreement suggested that the force field parameters

* Corresponding author. Tel.: +1-405-325-3502; fax: +1-405-325-6111.
E-mail address: rawheeler@chemdept.chem.ou.edu (R.A. Wheeler).

0032-3861/01/$ - see front matter © 2001 Published by Elsevier Science Ltd.
PII: S0032-3861(01)00234-8

reproduce well the crystalline PEO/PEO interactions. In subsequent MD work, analogues of PEO, C_2H_5-$O(-CH_2CH_2O-)_nC_2H_5$ with $n = 1$–9, 12, 15, 32, 65, 165, and 332, were simulated at 400 K to represent the pure melts [7]. The study showed that the dihedral angles along the C—O—C—C atom sequence favored the trans over the gauche conformation, while the gauche conformation dominated the dihedral angles along the O—C—C—O sequence. Lin et al. used a new procedure to generate PEO models by simulating the polymerization process of dimethyl ether in order to represent a multiply-dispersed sample of polymeric materials [8]. The authors reported structural and dynamical properties by presenting radial distribution functions and comparisons of calculated vibrational spectra with experiment. Poly(oxyethylene) (POE, $H(-CH_2CH_2O-)_nH$), has the same chain structure as PEO. A 12-repeat unit model of POE was simulated by Smith et al. at 300, 333, 373 and 450 K [9]. The mean square radii of gyration $\langle S^2 \rangle$ and end-to-end distances $\langle R^2 \rangle$ of this model agreed with small-angle neutron scattering (SANS) results for POE samples and followed the same temperature dependence. All the work above indicates that molecular dynamics simulations have become a fruitful approach to understand macromolecular structure.

Poly(ethylenimine) (PEI, $(-CH_2CH_2NH-)_n$) is an alternative to PEO because of their similar structures and ability to dissolve inorganic salts. In addition, the hydrogen atoms directly bonded to nitrogen add more complexity to PEI structures and give different ionic mobilities. The melting point for a semicrystalline PEI sample is 332 K and the glass transition temperature is 250 K [1]. The complexity of PEI structure is expected since the NH groups can behave as both hydrogen donors and acceptors. X-ray diffraction studies of linear PEI showed a different crystal structure than PEO. Chatani et al. revealed that the linear PEI chains adopt a double-stranded helical structure [10]. Each strand takes a (5/1) helical form and two strands are connected by inter-chain hydrogen bonds. In each NH group, the N and H atoms, as the hydrogen bond acceptor and the donor respectively, each form one H-bond with NH groups from another chain. The inter-atomic distance for N…N pairs is 3.16 Å. For each single chain, dihedral angles along the C—N—C—C backbone atom sequence are 160° and those along the N—C—C—N sequence are 13°. Intra-chain hydrogen bonds do not exist in the crystal structure.

Computer simulation is a good way to understand the structural characteristics of PEO, but to our knowledge there are no published MD results for models of PEI or PEI:salt complexes. In this work, we present our MD simulations on models of the amorphous phase of PEO and PEI at 300 K. Chain dimensions, dihedral angle distributions, and conformational triads population analyses are compared with each other. Radial distribution function analyses on the PEI model system are done to study the presence and the character of hydrogen bond structures.

2. Simulation methodology

2.1. Models

Low molecular weight oligomeric analogues of PEO have been widely used to model PEO and PEO:salt complexes as addressed in the introduction. Short oligomers can easily adopt a fully amorphous phase at accessible temperatures where ion transport takes place, so the structural analyses can be simplified by studying single-phase systems. Thus in this work, we use a four repeat-unit oligomer ($CH_3X(CH_2CH_2X)_4CH_3$, $X = O$ in PEO-4 and NH in PEI-4) as the simulation model for the single amorphous phase of PEO and PEI. For convenience, we shall call the tetramer models PEO-4 (it is conventionally called tetraglyme) and PEI-4. We filled PEO-4 and PEI-4 sample boxes with 50 chains and then simulated at 300 K, near room temperature. This is below the melting temperature but above the glass transition temperature for both PEO and PEI. This was done to obtain the amorphous phase in each.

2.2. Simulation details

The AMBER 5 computer program [11,12] was used for MD simulations. The initial configurations of PEO-4 and PEI-4 model molecules were generated by taking Cartesian coordinates of a PEO chain with the same length as the model molecules in the known crystal structure. The coordinates of oxygens were also used for nitrogens in PEI-4. The hydrogen in the NH groups was started along one tetrahedral direction with the correct N–H bond length. Periodic boundary conditions were applied and the SHAKE algorithm was used to constrain bond lengths, while bond angles and torsional angles remained flexible. The Berendsen coupling algorithm was used to maintain a constant temperature of 300 ± 30 K in the NPT and NVT ensembles [13] by scaling the kinetic energy every 10 ps. The particle mesh Ewald (PME) method [14] was used to calculate long-range electrostatic interactions with direct-space cutoff values of 10 Å for PEO-4 and 12 Å for PEI-4 [14]. Nonbonded interactions were truncated beyond these ranges. In all cases, the equations of motion were integrated by using the leap-frog version of the Verlet algorithm with a time step of 1 fs. The sample boxes of PEO-4 and PEI-4 were started at a density of 0.1 g/cm^3 and then simulated at 1 atmosphere for 1 ns in the NPT ensemble. Equilibrium densities for PEO-4 (1.0 g/cm^3) and PEI-4 (0.93 g/cm^3) were calculated by averaging densities over 0.2 ns. Calculated densities for PEO-4 and PEI-4 are close to experiment densities of PEO-4 and $H_2N(CH_2CH_2NH)_3CH_2CH_2NH_2$, which are 1.009 and 0.998 g/cm^3, respectively [15]. Further simulations were performed at 300 K in the NVT ensemble for 1.5 ns to reach equilibrium. To test for equilibration, total energies were monitored over the last 500 ps of the 1.5 ns run. The total energies fluctuated less than 1.6% and moving average energies calculated every 10 ps

increased less than 0.05% over the 500 ps for both systems. The cosine torsional angle autocorrelation function [16] was also calculated. For the C–C and C–O bonds in PEO-4, the relaxation times were 25.8 and 21.4 ps. In PEI-4, the relaxation times were 16.5 and 24.3 ps for the C–C and C–N bonds, respectively. After thus determining that our systems were at equilibrium, 500 ps of atomic trajectory data were collected for PEO-4 and PEI-4.

2.3. Force field parameters

The AMBER force field model uses a potential energy function composed of five different terms: harmonic bond length stretching, harmonic bond angle bending, sinusoidal dihedral angle twisting, a 6–12 Lennard–Jones interaction, and an electrostatic interaction [17]. A dielectric constant of unity is used in the electrostatic interaction term for both systems. The force field parameters used for PEO-4 are taken from the AMBER force field for ethers reported in the literature [17]. The force field parameters for the nitrogen atoms in PEI-4 were taken from a solvation free energy calculation on small aliphatic amines [18]. One missing parameter, the C—C—N bond angle bending force constant, is taken from a similar bond type in the database. The dihedral angle torsional parameter for the N—C—C—N atom sequence is obtained by fitting an energy profile from a density functional calculation of for dimethylethylenediamine (DMEDA) into the dihedral angle torsion functional form [19]. All parameters used in this study are given in Appendix A.

3. Results and discussion

The chain dimensions, dihedral angle distributions, and conformational triad populations were calculated and compared for PEO-4 and PEI-4 at 300 K based on their atomic trajectories. Radial distribution functions were used to probe hydrogen bonding structures for the PEI-4 system.

3.1. Chain dimensions

The overall polymer chain dimensions can be described by the mean square radius of gyration, $\langle S^2 \rangle$, and the mean square backbone end-to-end distance, $\langle R^2 \rangle$. The mean square radius of gyration, a weight averaged expression of polymer chain size, is a useful parameter in polymer studies because it can be measured directly by scattering methods. The characteristic ratio, defined as $C_n = \langle R^2 \rangle / nl^2$, where n is the number of backbone bonds and l^2 is the mean-square bond length, is theoretically predicted as 1 for a freely jointed polymer chain model of any length and is used to compare chain dimensions of polymer samples with different chain lengths [20]. A real polymer chain has a C_n value greater than 1 and it reaches a limit as n approaches ∞. For poly(oxyethylene) (POE, an analogue of PEO), the limiting value of C_n is approximately 5.2 [21]. Calculation results are listed in Table 1 for PEO-4 and PEI-4 at 300 K.

Table 1
MD results of mean-square radii of gyration, $\langle S^2 \rangle$, and end-to-end distances, $\langle R^2 \rangle$, and characteristic ratio, C_n, for PEO-4 and PEI-4 at 300 K

300 K	$\langle S^2 \rangle$	$\langle R^2 \rangle$	C_n
PEO-4	21.3 ± 0.3	143 ± 4	4.9 ± 0.1
PEI-4	17.7 ± 0.2	95 ± 3	3.1 ± 0.1

The characteristic ratio calculated in our work for PEO-4 is 4.9 ± 0.1. A small-angle neutron scattering (SANS) study on a nearly monodisperse POE sample gave the characteristic ratio as 5.7–5.5 in the temperature ranging of 347–459 K [9]. Another SANS result for a POE sample with a polydispersity of 1.5 at 353 K gave a value of 6.9 [22]. A characteristic ratio value for PEO with the molecular weight M_w from 6×10^3 to 1.1×10^7 in aqueous solution was reported to be 5.2 ± 0.1 at 298 K [23]. Our result for the monodisperse short chain sample is therefore in good agreement with the PEO C_n value, while it is smaller than the value for the monodispersed and polydispersed POE.

Smaller values of $\langle S^2 \rangle$ and $\langle R^2 \rangle$ for PEI-4 than for PEO-4 indicate a more compact spatial shape for PEI-4. The more compact shape in PEI-4 implies that there are relatively stronger intra-molecular attractions or inter-molecular repulsions within the PEI-4 sample. Experimental data for the characteristic ratio are lacking, so our MD result for PEI-4 cannot be compared to any experiment. A theoretical calculation of linear poly(ethylenimine), in which each dihedral angle was allowed to sample a small number of discrete torsional states according to the rotational isomeric state (RIS) theory, gave a value of 5.10–6.56 for the characteristic ratio at 300 K [24]. Our result of 3.6 ± 0.1 for PEI-4 is smaller than this theoretical prediction for the long chain PEI polymer.

3.2. Dihedral angle distribution

For the backbone atoms of PEO-4 and PEI-4 chains, there are two different types of dihedral angles defined by C—*X*—C—C and *X*—C—C—*X* atom sequences, where $X = O$ in PEO-4 and NH in PEI-4. In order to examine the conformations of PEO-4 and PEI-4 chains, the time-averaged population density distribution of these dihedral angles (θ) were calculated at 300 K and the results are plotted in Fig. 1.

Fig. 1(a) compares the population density distribution of dihedral angles along the C—*X*—C—C sequence in PEO-4 and PEI-4. By our definition, the conformations are eclipsed when $\theta = 0°$ and are labeled trans (denoted T) if $120° < \theta < 240°$, gauche plus (G^+) if $0° < \theta < 120°$, and gauche minus (G^-) if $240° < \theta < 360°$. Not surprisingly, these two dihedral angle types give a similar distribution because of the similarity of oxygen and NH groups. Both cases show that a trans conformation is predominant, while

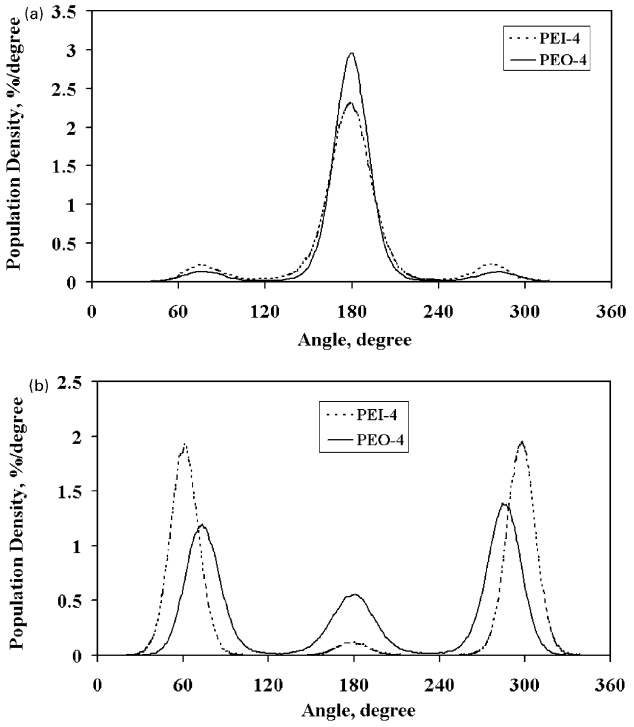

Fig. 1. (a) Average population density distribution of dihedral angles along the C—*X*—C—C backbone atom sequence for PEO-4 and PEI-4 at 300 K. (b) Average population density distribution of dihedral angles along the *X*—C—C—*X* backbone atom sequence for PEO-4 and PEI-4 at 300 K for both figures. $X = O$ in PEO-4 and NH in PEI-4.

gauche conformations (G^+ and G^-) give much smaller peaks near 80° and 280°, respectively. Neither G^+ nor G^- is favored. Moreover, PEO-4 shows a larger population of T (90%) while G^+ and G^- (10% total) are less populated compared to PEI-4 (T 84%, G 16%).

Fig. 1(b) is the population density distribution of dihedral angles along the *X*—C—C—*X* atom sequence for PEO-4 and PEI-4. The G^+ and G^- conformations are much more favored than T. This distribution is attributed to 'the gauche effect'. It is well accepted that when atoms at the two ends of a dihedral angle are very electronegative, the dihedral angle favors a gauche (G^+ or G^-) over the trans conformation despite the Coulombic repulsion between the two atoms [25]. The gauche effect has been found in high molecular-weight PEO and in lighter oligomeric crystals, melts, and solutions. By comparison, PEI-4 shows a more significant 'gauche effect' than PEO-4. In PEI-4, the dihedral angles are almost exclusively in the G^+ and G^- conformations (97% of the total compared to 78% in PEO-4), whereas the T (3%) conformation has a much lower population in PEI-4 than in PEO-4 (22%). The most favored dihedral angles of PEI-4 shift to 60 and 300°, toward the eclipsed conformation, compared to 75 and 285° in PEO-4. These significant differences suggest that there may be a force between the two NH groups other than the usual 'gauche effect' that pulls them closer. Hydrogen bonding is one likely possibility that will be described later.

3.3. Conformational triads population analysis

Conformational triads are a combination of three consecutive dihedral angles along the C—*X*—C—C—*X*—C atom sequence. The population analysis of triads is one way to examine local structures of polymers. In expressing the geometry of triads, G′ indicates a change in sign of the gauche conformation. For example, TGG′ corresponds either to the TG^+G^- or TG^-G^+ conformation. The result of the conformational triads analysis at 300K is shown in Fig. 2. In PEO-4, the TGT conformation has the largest population (59 ± 3%), with smaller, but still significant percentages of TTT (20 ± 2%) and TGG′ (10 ± 1%) triads. The result qualitatively agrees with an MD simulation on monoglyme and diglyme in aqueous solutions at 318 K [26], for monoglyme:water and diglyme:water mole fractions of 0.004–0.180 and 0.004–0.130, respectively. This study reported 60–70% TGT populations. In PEI-4, the TGT conformation is even more favorable (66 ± 2%) than in PEO-4. Among all conformations, the largest differences in populations between PEO-4 and PEI-4 are TGG (24 ± 1% in PEI-4 and 6 ± 2% in PEO-4) and TTT (1.6 ± 0.4% in PEI-4 and 20 ± 2% in PEO-4). The different TGT and TTT populations are understandable, since the dihedral angle distribution analysis shows that the central dihedral angle of triads along the N—C—C—N sequence favors the gauche over the trans conformation much more in PEI-4 compared to PEO-4.

3.4. Radial distribution function analysis for PEI-4

Radial distribution function (RDF) calculations provide insights into the PEO-4 and PEI-4 structures by reporting the relative density of atom pairs separated by a distance *r*:

$$g(r) = \frac{V}{N^2}\left\langle \sum_i \sum_{j \neq i} \delta(r - r_{ij}) \right\rangle$$

where *i* and *j* refer to the *i*th and *j*th molecules and the angle

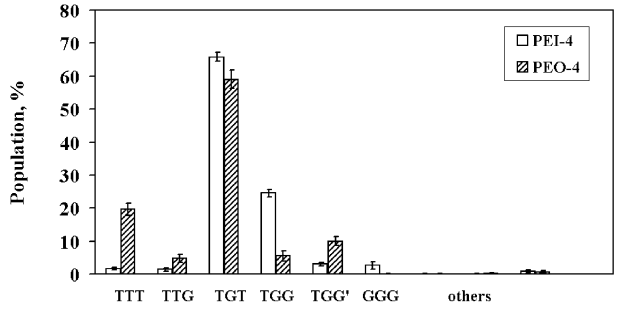

Fig. 2. Population analysis of conformational triads along the C—*X*—C—C—*X*—C backbone atom sequence for PEO-4 and PEI-4 at 300 K. $X = O$ in PEO-4 and NH in PEI-4. The standard deviations are shown as error bars.

brackets imply averaging over different configurations [27]. These functions give a way to infer interactions between atoms. Smith et al. reported the pair radial distribution functions for POE models [9]. Our calculation gives similar results, so they are not addressed here. The PEI system, with its NH group instead of the ether oxygen in PEO, has more interesting structural characteristics. As discussed in the introduction, the NH group is key to forming hydrogen bonding interactions.

We have chosen to focus on three possible ways to form a hydrogen bond between the two NH groups, depending on their relative positions. Adjacent NH groups are separated by one ethyl group, non-adjacent groups are separated by at least two ethyl groups but are in the same molecule, and intermolecular NH groups are from different molecules. All those component RDFs and the total RDF between nitrogen and hydrogen atoms (N…H) and between two hydrogen atoms (H…H) are plotted in Figs. 3 and 4. The hydrogen atoms are only those within NH groups and, in the adjacent RDF calculation, the hydrogen and nitrogen pair that forms a covalent bond is omitted.

The intermolecular RDFs are plotted in Figs. 3 and 4 to examine intermolecular hydrogen bonding. The non-adjacent N…H and H…H RDFs only show very small and indistinct structure in Figs. 3 and 4. This result indicates that minimal non-adjacent hydrogen bonding occurs. In Fig. 3, the first peak of the intermolecular N…H RDF occurs at 2.3 Å. The intermolecular N…N RDF (not shown) gives 3.3 Å as the most probable distance, as compared to the twice van der Waals distance of 3.75 Å for nitrogen atoms. Since the covalent bond length of N–H is 1.01 Å and the N…H distance is 2.3 Å, the intermolecular hydrogen bonding is linear. Thus, H-bonds with the classical 180° N–H…N angle, N…H distances near 2.3 Å, and N…N distances less than the sum of van der Waals radii are formed between different PEI-4 chains. The populations of a single PEI-4 chain connected with other chains by

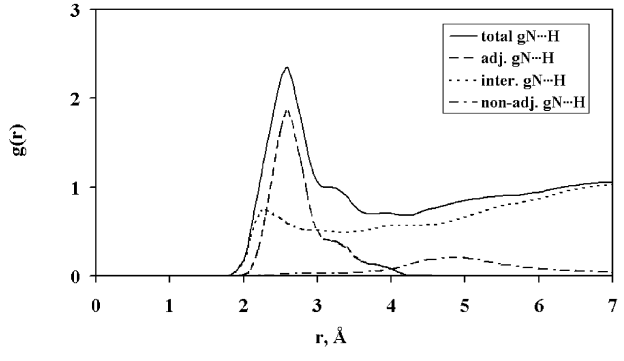

Fig. 3. The total radial distribution functions (RDFs) of N…H pairs and its components for PEI-4 at 300 K. The adjacent (NH groups are separated by one ethyl groups), non-adjacent (NH groups are separated by at least two ethyl groups but are in the same molecule), and intermolecular (NH groups are from different molecules) RDF are represented as dashed, dash dotted, and dotted lines, respectively. Only hydrogen atoms in NH groups are considered.

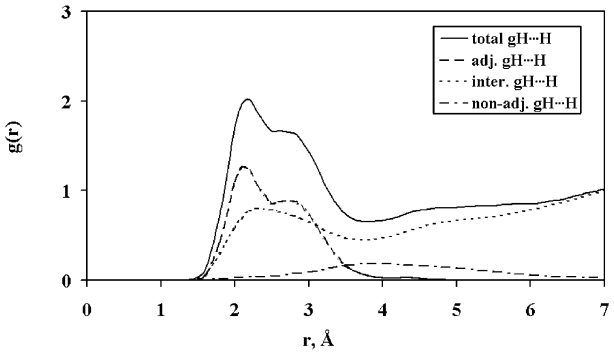

Fig. 4. The total radial distribution functions of H…H pairs and its components for PEI-4 at 300 K. The adjacent, non-adjacent, and intermolecular RDF are represented as dashed, dash dotted, and dotted lines, respectively. Only hydrogen atoms in NH groups are considered. The adjacent RDF clearly shows two peaks at 2.2 and 2.8 Å implying two distinguishable structures. These structures are shown in Fig. 5 labeled (A), double H-bonding for the first peak, and (B), single H-bonding structure for the second peak. The first minimum between the first and second peak, at 2.55 Å, is set as the cutoff to distinguish the two structures.

hydrogen bonding were calculated. The most common case (39.0%) is that of a single PEI-4 chain that hydrogen bonds to only one other chain. Single chains which hydrogen bond to two or three chains also have large populations (38.1 and 13.8%). The population for chains having no hydrogen bonds with others is only 7.0%. But this intermolecular N…H RDF does not account for the majority of the total RDF. It implies that intermolecular H-bonding is not the most favorable structure.

We now analyze the extent of H-bonding between NH groups separated by only one ethyl group. In Fig. 3 the adjacent N…H RDF shows a strong peak at 2.6 Å, with a distinct shoulder near 3.3 Å. This peak implies an attraction between the nitrogen and hydrogen, but the distance is not short enough to represent a classical hydrogen bond, whose N…H distance is approximately 2.0 Å [28]. The peak position in the adjacent N…H RDF is slightly longer than 2.3 Å, the most probable length of an intermolecular H-bond. Because the adjacent NH pairs have to overcome the restraint of bond angles, the N…H distances between adjacent NH pairs cannot get as close as those between different molecules. For convenience, we shall not distinguish this hydrogen-bond-like interaction between adjacent NH groups from classical hydrogen bonding. It can explain the dihedral angle distribution of PEI-4, as it stabilizes the gauche conformations for dihedral angles along N—C—C—N. It also causes the shift of these dihedral angles toward the eclipsed geometry, relative to PEO-4, because the two NH groups can get closer to each other. The presence of the shoulder (3.3 Å) is an interesting feature and its origin is described later.

Fig. 4 shows H…H RDFs for PEI-4. As in Fig. 3, the total RDF has the same shape as the RDF for hydrogens in adjacent NH groups in the distance range below 4 Å. There are two peaks that occur at 2.2 and 2.8 Å, separated

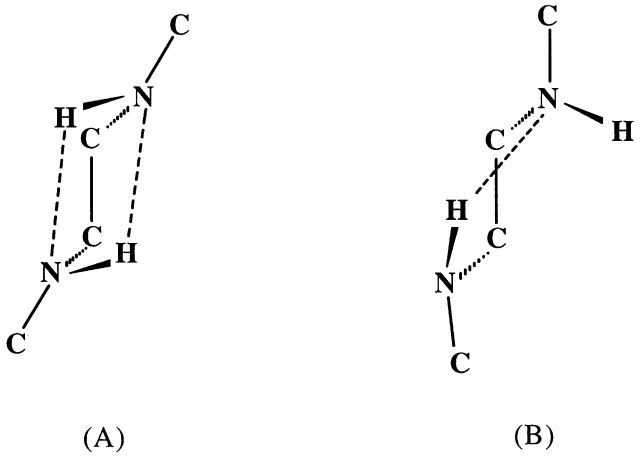

Fig. 5. Diagrams of two distinguishable H-bonding structures in (NH)—C—C—(NH) units in PEI-4. (A) Double H-bond and (B) single H-bond.

by a shallow minimum at 2.55 Å. This means there are two distinguishable (NH)—C—C—(NH) structures. Since 97% of the dihedral angles along this atom sequence are in a gauche conformation, there are two distinguishable gauche conformations. (They are not G^+ and G^- because G^+ and G^- are statistically indistinguishable.) A number of local structures have been examined for adjacent H…H distances of 2.2 and 2.8 Å to identify typical structures. Two distinguishable gauche structures were found. One is a double hydrogen bonding structure in which both N–H bonds are oriented toward the adjacent nitrogens (see Fig. 5(A)). The structure is symmetrical and the distance between the two hydrogen atoms is near 2.2 Å, so this corresponds to the first peak in the adjacent H…H RDF. Conformational constraints prevent the two N–H bonds from pointing directly at the adjacent nitrogen to form a 180° N–H…N angle. In the other structure, one of the hydrogen atoms points toward the adjacent nitrogen and one points away from the adjacent nitrogen (Fig. 5(B)). The distance between the two hydrogen atoms on adjacent nitrogen atoms is 2.8 Å, which gives the second peak in the adjacent H…H RDF. Once again, the N–H…N angle of this structure cannot be 180°. A third gauche structure without H-bonds is also possible with both H atoms pointing away from the adjacent N atoms. In this case, the H…H distance would be longer than that in either the singly or the doubly hydrogen bonded structures. The absence of any peaks in the adjacent H…H RDF at longer distances than 2.8 Å suggests that the TGT conformation without H-bonding is unfavorable.

Referring back to the shoulder of the adjacent N…H RDF at 3.3 Å in Fig. 3, the double hydrogen bonding structure, structure (A), cannot cause this feature since its N…H distance is too short. The single hydrogen bonding structure, structure (B), could cause this shoulder because there is one non-H-bonded N…H pair in this structure and this explanation is verified by Fig. 6. Fig. 6 shows the contributions from the structures in Fig. 5(A) and (B) to the adjacent N…H

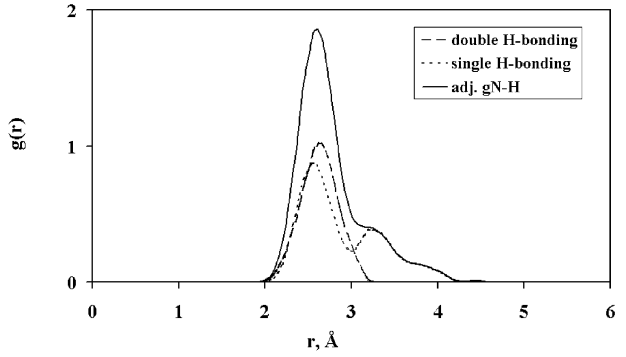

Fig. 6. The contributions from the double H-bonding and the single H-bonding structure to the adjacent N…H RDF.

RDF. The cutoff value for distinguishing the two structures is set at 2.6 Å, the minimum between the first and second peak in the adjacent H…H RDF. If the H…H distance is less than 2.6 Å, the structure is considered to adopt structure (A), and the N…H RDF is calculated to give its contribution to the total adjacent N…H RDF. The same procedure is repeated for structure (B) where the H…H distance is greater than 2.6 Å. In Fig. 6, the different shapes of the two structural contributions to the RDF are clearly shown. The single peak in the contribution from structure (A) implies that the two hydrogen bonds are formed approximately within the same distance, 2.6 Å. Thus, the structure is symmetrical. The split contribution from structure (B) shows its asymmetrical character in the relative positions of N and H. The first peak at 2.6 Å is the length of the H-bond and the second peak at 3.3 Å is the distance between the non-H-bonded N…H pair. Thus, based on analyses of the adjacent N…H and H…H RDFs, we conclude that there are two distinguishable H-bonding structures responsible for the predominance of the gauche conformation of the (NH)—C—C—(NH) angle, the double and the single hydrogen bonding structures. An integration of the adjacent H…H RDF gives relative populations of the two structures as 37% double H-bond and 63% single H-bond structures.

Hydrogen-bonding angle distributions for the structures (A) and (B) are calculated and plotted in Fig. 7. Each structure

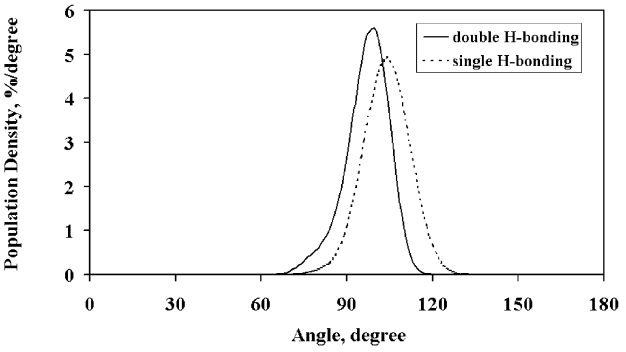

Fig. 7. The H-bond angle distribution for the double H-bonding and the single H-bonding structures.

simply gives one peak, at 99° for structure (A) and 104° for (B). The values indicate that the adjacent H-bond is far from linear, probably because of conformational constraints of the chain.

The mean lifetime of the adjacent H-bonding was also calculated to ensure that our results are statistically meaningful. In Fig. 6, the first minimum of the adjacent N…H RDF occurs at 3.0 Å and any N…H pairs within this distance will be considered to form H-bonds. The H-bonds will be considered to break when the N…H distances become larger than 3.0 Å. The calculation gives a time much shorter that the 500 ps length of the trajectory, 11.4 ps, as the mean H-bond lifetime.

The MD results demonstrating hydrogen bonding structures between adjacent NH groups is consistent with an ab initio study of dimethylethylenediamine (CH_3-NH—CH_2—CH_2-NH—CH_3, DMEDA) [19]. This work implies that the TGT structure is the most stable and also gives the single H-bonding structure as the lowest energy structure and the double H-bonding structure as the second lowest energy from among eight different structures calculated. This agrees qualitatively with our populations of the two structures (63% for single and 37% for double). The ab initio double H-bonding structure gives N…H distances of 2.59 Å, H…H distances of 2.20 Å, and the N–H…N angles of 95.0° close to our MD results of 2.6 Å, 2.2 Å and 99°, respectively. The ab initio single H-bonding structure gives N…H distances of 2.45 and 3.31 Å, H…H distances of 2.85 Å, and N–H…N angles of 107.4°. Once again, our MD results of 2.6, 3.3, 2.8 Å, and 104° agree closely with values from ab initio quantum chemistry.

3.5. Helical structure analysis of PEO-4 and PEI-4 chains

The dihedral angle distribution and the conformational triads population analysis of PEO-4 and PEI-4 provide information regarding their local structures. Recall that PEO and PEI crystal structure both show long-range conformational order: PEO chains adopt a (7/2) single helical [5], while PEI chains adopt a (5/1) double-stranded helical structure [10]. Inter-chain H-bonding stabilizes the tightly formed double helix of crystalline PEI. In the amorphous state, it is not known how much of the helical structure may be retained. Since crystalline PEO executes two helical turns for every seven repeat units, four monomeric units plus end-capping methyl and methoxy groups are sufficient for PEO-4 to form one helical turn. Likewise crystalline PEI executes one helical turn every five monomer units but adopts a double helical structure. Since our calculations imply that PEI-4 is more compact than PEO-4, four monomeric units plus the end-caps should be sufficient to form locally helical structures for PEI-4. Our results show, however, that only small parts of PEO-4 (5.6%) and PEI-4 (8.2%) adopt helical structures, with left- and right-handed helices being equally populated. For PEI-4, calculations indicate that the single H-bonding is favored over the double H-bonding structure within helices.

The intermolecular H-bonding analysis can indicate the extent of double-stranded helical structure in PEI-4. For our four repeat unit PEI model, a double helix extending the entire length of one chain requires eight H-bonds exclusively with one other chain. Our result implies that only 2.0% of the total PEI-4 chains adopt this structure. So very little double stranded helical structure exists in the amorphous state of PEI-4.

4. Conclusions

Molecular dynamics simulations of four repeat unit models of poly(ethylene oxide) (PEO) and poly(ethylenimine) (PEI), denoted PEO-4 and PEI-4, were performed at 300 K. The chain dimensions, dihedral angle distributions, and conformational triad populations were calculated and compared with available experiments to show the similarities and differences between equilibrium amorphous structures of PEO-4 and PEI-4.

The chain dimension calculations gave values of the mean-square radius of gyration, $\langle S^2 \rangle$, and mean-square end-to-end distance, $\langle R^2 \rangle$, both measures of spatial extent of a polymer, for the two systems. The $\langle S^2 \rangle$ value of 17.7 ± 0.2 and $\langle R^2 \rangle$ value of 95 ± 3 for PEI-4 are smaller than the corresponding values for PEO-4, 21.3 ± 0.3 and 143 ± 4, and indicate a more compact form for amorphous PEI-4 at 300 K. The characteristic ratio is 4.9 ± 0.1 for PEO-4 and 3.1 ± 0.1 for PEI-4 and are comparable to results from small-angle neutron scattering experiments [9,22], other MD simulations [9], and theoretical predictions [24] for similar systems related to PEO-4.

The dihedral angle distribution analysis reveals that PEO-4 and PEI-4 have similar distributions for the two types of dihedral angles, C—*X*—C—C and *X*—C—C—*X* (*X* = O in PEO-4 and NH in PEI-4). The C—*X*—C—C dihedral angles favor a trans conformation (T) while the gauche conformation (G^+ and G^-) is predominant for the *X*—C—C—*X* dihedral angles. For the C—*X*—C—C dihedral angles, PEO-4 has 90% T conformations and 10% G^+ and G^- compared to 84% T and 16% G^+ and G^- conformations for PEI-4. For the *X*—C—C—*X* dihedral angles, PEI-4 almost exclusively favors G^+ or G^- conformations (97% population). By comparison, 78% of the *X*—C—C—*X* dihedral angles in PEO-4 adopt G^+ and G^- conformations. The most probable angles for G^+ or G^- conformations are also different. In PEO-4, they are 75 and 285° while in PEI-4 they shift to 60 and 300°. The large populations of G^+ or G^- and the shift of the most probable dihedral angles toward a more eclipsed conformation suggest a stronger attraction between the adjacent NH groups in PEI-4.

A triad population analysis implies that the TGT conformation is the most stable local structure for PEO-4 and PEI-4 because of its large population ($59 \pm 3\%$ in PEO-4

and 66 ± 2% in PEI-4). PEO-4 shows a secondary preference for TTT conformations (20 ± 2%) and PEI-4 has secondary preference for TGG conformations (24 ± 1%). The TTT conformer is negligibly populated (1.6 ± 0.4%) in PEI-4. It is easy to understand the decrease of the TTT population in PEI-4 because only 3% of N—C—C—N dihedral angles adopt the T conformation.

The presence of NH groups in PEI-4 brings more complexities to its structure. One of the most important features is the possibility of hydrogen bond formation, since the NH groups can behave as both hydrogen bond donors and acceptors. Total radial distribution functions (RDFs) and their component adjacent, non-adjacent, and intermolecular RDFs were calculated for N…H, H…H, and N…N pairs of PEI-4. Two distinguishable hydrogen bonding structures between adjacent NH groups have been found. One is the double H-bonding structure in which each member of an NH pair acts as an H-bond donor and acceptor to the other adjacent NH of the pair (Fig. 5(A)). Another is the single H-bonding structure in which only one NH group forms an H-bond with an adjacent N (Fig. 5(B)). In both cases the H-bonds are long (N…H distances are 2.6 Å for both), and non-linear (N–H…N angles are 99° for the double H-bond and 104° for the single). The single H-bonding structure is more prevalent (63%) than the double (37%) and is apparently the most stable local structure for the (NH)—C—C—(NH) unit.

Intermolecular hydrogen bonding was examined by analyzing the intermolecular N…H RDF for PEI-4. Its small contribution to the total N…H RDF suggests that intermolecular H-bonding is not as common as H-bonding between adjacent NH groups in the same chain, but the shorter N…H distance implies that this interaction is stronger than the adjacent H-bonding. The RDF results also show that the intermolecular H-bonding structure is nearly linear.

Only a small percentage of PEO-4 and PEI-4 adopt a helical structure (5.6% for PEO-4 and 8.2% for PEI-4). This means that PEO-4 and PEI-4 chains are much less ordered than in the polymer crystalline phases, where PEO is helical and PEI adopts a double helical structure. A population analysis of PEI-4 chains displaying intermolecular H-bonds was done to test the existence of double-stranded helices. The result indicates that this structure exists to an insignificant degree in the amorphous state of PEI-4 at 300 K.

Acknowledgements

We are grateful to the National Science Foundation/ National Resource Allocations Committee for a supercomputer time award at the University of Illinois (award number MCA96-N019 to R.W.) and to the NSF for financial support for Curtis Durham (NSF-REU# CHE-9820544). We thank Professor Daniel T. Glatzhofer for administering the REU/SURF program, Scott E. Boesch for providing force field parameters for torsions of the PEI-4 chain and for sharing results of his quantum chemical calculations, and an anonymous reviewer for clarifying several issues concerning characteristic ratios.

Appendix A

The potential energy function used to describe simulation models is:

$$E_{\text{total}} = \sum_{\text{bonds}} K_r(r - r_{\text{eq}})^2 + \sum_{\text{angles}} K_\theta(\theta - \theta_{\text{eq}})^2 + \sum_{\text{dihedrals}} \frac{V_n}{2}[1 + \cos(n\phi - \gamma)] + \sum_{i<j}\left[\frac{A_{ij}}{R_{ij}^{12}} - \frac{B_{ij}}{R_{ij}^{6}}\right] + \sum_{i<j}\frac{q_i q_j}{\epsilon R_{ij}}$$

All parameters for PEO-4 and PEI-4 are listed in Tables A1 and A2. Note that $A_{ij} = \epsilon^*(R^*_{ij})^{12}$ and $B_{ij} = 2\epsilon^*(R^*_{ij})^6$ in the van der Waals parameter section.

Table A1
Force field parameters for PEO-4 [13]

	Bond parameters			
Bond	K_r (kcal/molÅ^2)	r_{eq} (Å)		
CT-CT	310.0	1.526		
CT-HC	340.0	1.090		
CT-OS	320.0	1.410		
	Angle parameters			
Angle	K_θ (kcal/mol rad^2)	θ_{eq} (deg)		
CT-CT-HC	50.0	109.50		
CT-CT-OS	50.0	109.50		
CT-OS-CT	60.0	109.50		
HC-CT-HC	35.0	109.50		
	Torsional parameters			
Torsion	No. of paths	$V_n/2$ (kcal/mol)	γ (deg)	n
X-CT-CT-X	9	1.40	0.0	3.0
X-CT-OS-X	3	1.15	0.0	3.0
CT-CT-OS-CT	1	0.383	0.0	−3.0
CT-CT-OS-CT	1	0.1	180.0	2.0
OS-CT-CT-OS	1	0.144	0.0	−3.0
OS-CT-CT-OS	1	1.00	0.0	2.0
	van der Waals parameters			
Atom type	R^* (Å)	ϵ^* (kcal/mol)		
CT	1.9080	0.1094		
HC	1.4870	0.0157		
OS	1.6837	0.1700		

Table A2
Force field parameters for PEI-4

	Bond parameters			
Bond	K_r (kcal/molÅ^2)	r_{eq} (Å)		
CT–NT [14]	367.0	1.471		
NT–HN [13]	434.0	1.010		
	Angle parameters			
Angle	K_θ (kcal/mol rad^2)	θ_{eq} (deg)		
CT–CT–NT [13]	80.0	111.20		
CT–NT–HN [14]	35.0	109.50		
CT–NT–CT [14]	60.0	109.50		
HC–CT–NT [14]	35.0	109.50		
	Torsional parameters			
Torsion	No. of paths	$V_n/2$ (kcal/mol)	γ (deg)	n
X–CT–NT–*X* [14]	6	1.0	0.0	3.0
NT–CT–CT–NT [15]	1	0.6	0.0	−3.0
NT–CT–CT–NT	1	0.4	0.0	−2.0
NT–CT–CT–NT	1	0.6	180.0	1.0
	van der Waals parameters			
Atom type	R^* (Å)	ϵ^* (kcal/mol)		
NT [T14]	1.875	0.1700		
HN [N14]	1.689	0.0157		

References

[1] Tanaka R, Fujita T, Nishibayashi H, Saito S. Solid State Ionics 1993;60:119.
[2] Berthier C, Gorecki W, Minier M, Armand MB, Chabagno JM, Rigaud P. Solid State Ionics 1983;11:91.
[3] Armand MB, Chabagno JM, Duclot M. Second International Meeting on Solid Electrolytes. St Andrews, Scotland. 1978:Extented Abstract.
[4] MacCallum JR, Vincent CA. Polymer electrolyte reviews, vol. 1. New York: Elsevier, 1987.
[5] Takahashi Y, Tadokoro H. Macromolecules 1973:672.
[6] Neyertz S, Brown D, Thomas JO. J Chem Phys 1994;101:10064.
[7] Neyertz S, Brown D. J Chem Phys 1995;102:9275.
[8] Lin B, Boinske PT, Halley JW. J Chem Phys 1996;105:1668.
[9] Smith GD, Yoon DY, Jaffe RL, Colby RH, Krishnamoorti R, Fetters LJ. Macromolecules 1996;29:3462.
[10] Chatani Y, Kobatake T, Tadokoro H. Macromolecules 1982;15:170.
[11] Case DA, Pearlman DA, Caldwell JW, Cheatham III TE, Ross WS, Simmerling CL, Darden TA, Merz KM, Stanton RV, Cheng AL, Vincent JJ, Crowley M, Ferguson DM, Radmer RJ, Seibel GL, Singh UC, Weiner PK, Kollman PA. AMBER 5; University of California-San Francisco: San Francisco. 1997.
[12] Pearlman DA, Case DA, Caldwell JW, Ross WS, Cheatham III TE, DeBolt S, Ferguson D, Seibel G, Kollman P. Comp Phys Comm 1995;91:1.
[13] Berendsen HTC, Postma JPM, van Gunsteren WF, DiNola A, Haak JR. J Chem Phys 1984;81:3684.
[14] Darden T, York D, Pedersen L. J Chem Phys 1993;98:10089.
[15] Aldrich Handbook, 2000–2001. p. 1560.
[16] McQuarrie DA. Statistical Mechanics. New York: Harper & Row, 1976.
[17] Cornell WD, Cieplak P, Bayly CI, Gould IR, Merz KM, Ferguson DM, Spellmeyer DC, Fox T, Caldwell JW, Kollman PA. J Am Chem Soc 1995;117:5179.
[18] Morgantini P, Kollman PA. J Am Chem Soc 1995;117:6057.
[19] Boesch SE, York SS, Frech R, Wheeler RA. J Chem Soc, Phys Chem Comm 2001. 1. Electronically published at http://www.rsc.org/is/journals/current/physchemcomm/pccpub.htm.
[20] Flory PJ. The statistical mechanics of chain molecules. New York: Hanser, 1988.
[21] Abe A, Furuya H, Mitra MK, Hiejima T. Comput Theor Polym Sci 1998;8:253.
[22] Kugler J, Fischer EW, Peuscher M, Eisenbach CD. Makromol Chem 1983;184:2325.
[23] Kawaguchi S, Imai G, Suzuki J, Miyahara A, Kitano T, Ito K. Polymer 1996;38:2885.
[24] Wang S, DeBolt L, Mark JE. Polym Prepr 1993;34:478.
[25] Abe A, Mark JE. J Am Chem Soc 1976;98:6468.
[26] Bedrov D, Borodin O, Smith GD. J Phys Chem B 1998;102:5683.
[27] Allen MP, Tildesley DJ. Computer simulation of liquids. New York: Oxford University Press, 1987.
[28] Schuster P, Zundel G, Sandorfy C. The hydrogen bond: recent developments in theory and experiments, vol. 2. Amsterdam: North-Holland Publishing Company, 1976.